TITLE

NAME Three-Dimensional (3-D) Low-Resolution S-Pol Radar Grids, Version 1
Last Updated 20 April 2007

AUTHORS

Timothy J. Lang
Department of Atmospheric Science
Colorado State University
200 W Lake St
Fort Collins, CO 80523
tlang@atmos.colostate.edu
(970) 491-6944

Steven A. Rutledge, PI
CSU Atmospheric Science
rutledge@atmos.colostate.edu

Rit Carbone, PI
NCAR
carbone@ucar.edu

Refer data questions to Timothy Lang

1.0 DATA SET OVERVIEW

This README assumes some basic understanding of meteorological radars, in particular Doppler and polarimetric radars. If you need more complete radar references, the Battan (1973), Doviak and Zrnic (1993), and Bringi and Chandrasekar (2000) textbooks are recommended.

This dataset includes three-dimensional grids of standard polarimetric radar fields from the S-Pol radar – part of the NAME radar network, which consisted of three radars located near the mouth of the Gulf of California and the western slope of the Sierra Madre Occidental. The locations of these radars are shown in Fig. 1.

The three radars are:
1. S-Pol – 23.9290 N, 106.9521 W, 20 m MSL
2. Cabo – 22.8971 N, 109.9272 W, 281 m MSL
3. Guasave – 25.5676 N, 108.4633 W, 85 m MSL

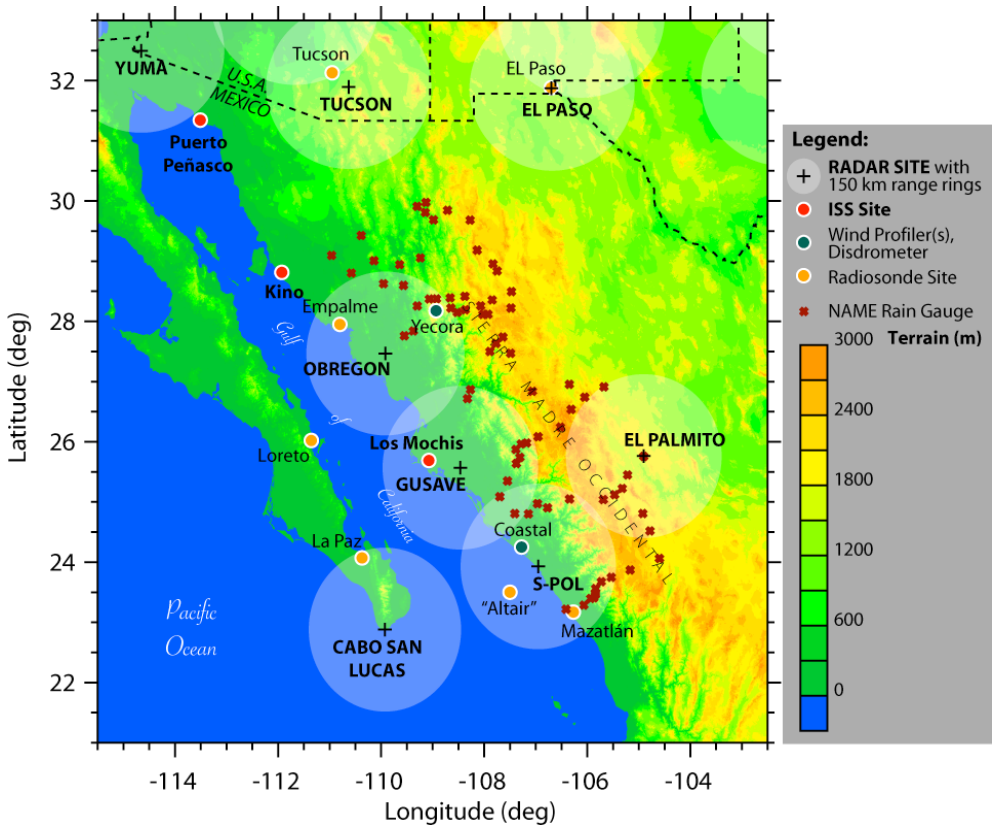

Figure 1. Locations of radars and other instrument sites during NAME 2004. Plot courtesy of NAME community.

The Version 1 grids cover the period 7/8 0000 UTC thru 8/21 2345 UTC. The temporal resolution is 15 minutes. Significant gaps in radar coverage occurred during this time – too many to ennumerate. Refer to the files themselves to identify when grids are available.

2.0 INSTRUMENT DESCRIPTION

Meteorological Radar
S-Pol: S-band, Doppler, polarimetric (linear H & V polarizations), 1.0° beamwidth

The S-Pol radar was run at two main PRFs, 720 Hz and 960 Hz. 720 Hz was the most common and provided an unambiguous range of ~210 km. 960 Hz was less common and provided a range near 150 km. Some other PRFs were used occasionally, especially early in the NAME EOP. These ranged between 720 and 1000 Hz.

S-Pol collected data usually between 0.5/0.8° up to 14.0° elevation. When echoes were closer, we coarsened the resolution and collected data up to 26.4°.

3.0 DATA COLLECTION AND PROCESSING

INTRODUCTION

Prior to creation of the 3-D grids, all S-Pol radar data were subjected to vigorous quality control efforts.

S-Pol is an S-band polarimetric Doppler radar that was located near La Cruz in Sinaloa. It was available 7/8-8/21 during 2004. Version 1 grids contain data from 7/8 onward.

Reflectivity (Z_H) and differential reflectivity (Z_{DR}) calibration biases were corrected by NCAR/EOL prior to any further QC efforts.

Due to the availability of polarimetric variables, we were able to automate most of the quality control for S-Pol. The goal was to eliminate clutter/AP, noise, second-trip echo, and insect echo. In order to accomplish this, the following filters were applied to all PPI swps:

ρ_{HV} – Range-based filter; We removed data with correlation coefficient (ρ_{HV}) < 0.8, except for range > 90 km and Z_H > 20 dBZ. For those data, we only eliminated gates with ρ_{HV} < 0.5 (noise/clutter).

SD(Φ_{DP}) – We calculated standard deviation of differential phase, SD(Φ_{DP}), over a moving window of 11 gates (1.65 km) and eliminated any data where SD > 18° if Z_H > 35 dBZ. If Z_H < 35 dBZ, we eliminated data where SD > 10° (noise/clutter).

LDR/Φ_{DP} – We eliminated data where linear depolarization ratio (LDR) > –5.0 and Φ_{DP} > 30° (second-trip).

Z_H/Z_{DR} – We eliminated all data where Z_H < 0 dBZ. For Z_H between 0 and 10 dBZ, we eliminated data where Z_{DR} > 1 dB. For Z_H between 10 and 35 dBZ, we eliminated data where $Z_{DR} > 1+0.075*Z_H$ (noise/insects).

The S-Pol test pulse was removed in an automated matter by eliminating the last several gates where it was usually located. This position varied with PRF. Occasionally, the test pulse was located elsewhere, and had to be removed by hand using soloii.

Φ_{DP} was filtered using a 21-gate (3.15-km) finite impulse response filter developed by John Hubbert of NCAR and V. N. Bringi of Colorado State University. Small data gaps within this moving window were filled using linear interpolation, in order to increase the amount of usuable windows for subsequent specific differential phase (K_{DP}) calculation. K_{DP} was calculated from the slope of a line fitted to the filtered Φ_{DP} field. The window over which this line was fitted changed depending on the Z_H of the central gate. If Z_H < 35 dBZ, then we fitted to 31 gates (4.65 km). For Z_H between 35 and 45 dBZ, we fitted to 21 gates (3.15 km). For Z_H > 45 dBZ, we fitted to 11 gates (1.65 km). This allowed for more accurate K_{DP} estimates at both high and low Z_H. For a handful of sweeps during a major storm on 8/3, we found that Φ_{DP} became folded due to the large areas of intense rain. Prior to filtering and K_{DP} estimation, we unfolded the Φ_{DP} field by hand using soloii.

Z_H and Z_{DR} were corrected for differential attenuation based on examining the behavior of these variables as a function of Φ_{DP} for a given range of K_{DP} values. In this situation, we found that both Z_H and Z_{DR} decreased with increasing phase shift, due to attenuation by liquid water. Lines were fitted to these relationships, and the slopes were used to correct Z_H and Z_{DR} as Φ_{DP} increased above 0°. An example for Z_H is shown in Fig. 2. The coefficient (slope) used for Z_H was 0.0171 dBZ $^{\circ -1}$. The Z_{DR}-Φ_{DP} relationship was noisy. The fitted slope was 0.0048 dB $^{\circ -1}$, but due to the scatter in this relationship, we used the Z_{DR} correction coefficient from the TRMM-LBA project in 1999, which was 0.0042. For 100° of phase shift (common in strong MCS convection), we would correct Z_H by +1.71 dBZ and Z_{DR} by +0.42 dB.

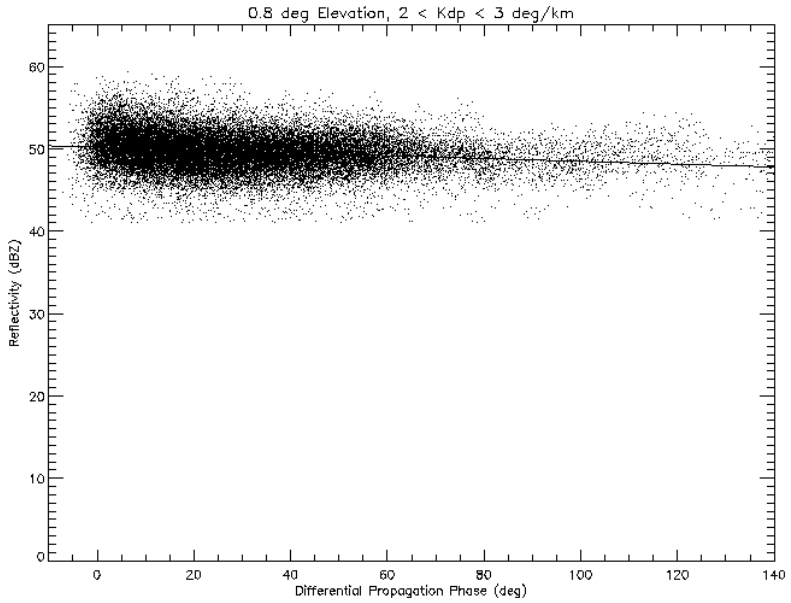

Figure 2. Scatterplot of Z_H vs. filtered Φ_{DP} for the specified K_{DP} range, using one week of S-Pol data from NAME. Also shown is the linear fit to the data.

Z_H was further corrected for gaseous attenuation. We used the established value of 0.007 dBZ km^{-1} (Battan 1973). This has to be doubled for a given range since the radar beam travels to and from the target. The correction at 200 km is +2.8 dBZ.

Despite all the thresholds, some clutter and insect echo remained after automated filtering. These remaining spurious echoes were subsequently removed by hand with soloii. In addition, we despeckled the data using the soloii algorithm. This removed any echo that contained only 2 or fewer contiguous gates.

Figure 3 shows an example of the beam blockage observed at S-Pol during NAME 2004. Significant amounts of beam blockage occured in S-Pol's NE sector (351-105° azimuth). This blockage was caused by mountain peaks intercepting the radar beam at low elevation angles. The location of the blocks was determined to the nearest degree in azimuth and nearest km in range by visual inspection of clear-air radar sweeps. Then, within rainfall (identified by the CSU hydrometeor identification or HID algorithm;

Tessendorf et al. 2005) in the blocked regions, we examined the behavior of Z_H as a function of azimuth for a given K_{DP} range. Because there were sometimes multiple blocks along the same ray, we had to do this analysis for both exterior (Fig. 4) and interior (Fig. 5) ranges, the values of which varied as functions of azimuth and reflected the locations of the blocks. However, we never examined data within 20 km of S-Pol. Due to the self-consistency between polarimetric variables, for a given range of K_{DP}, Z_H should vary only over a small range as well. If Z_H drops significantly below this range, that signals a block. The difference in the median Z_H values in unblocked regions, and median Z_H values in a blocked ray, is the +dBZ correction that needs to be applied to Z_H.

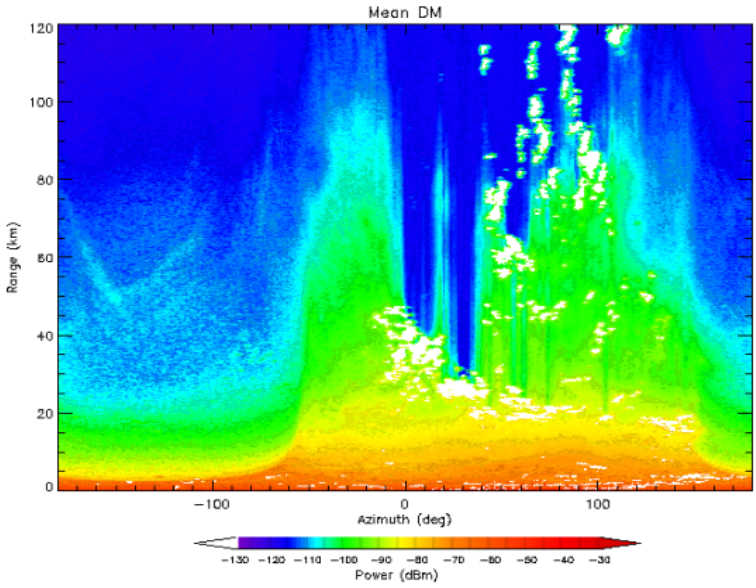

Figure 3. Average power return for 12 h of clear air returns at S-Pol. Blocks show up as significant reductions in mean power in the azimuths -9° (351°) to 105°. Clutter is flagged in white. Note that there were sometimes multiple blocks along the same ray.

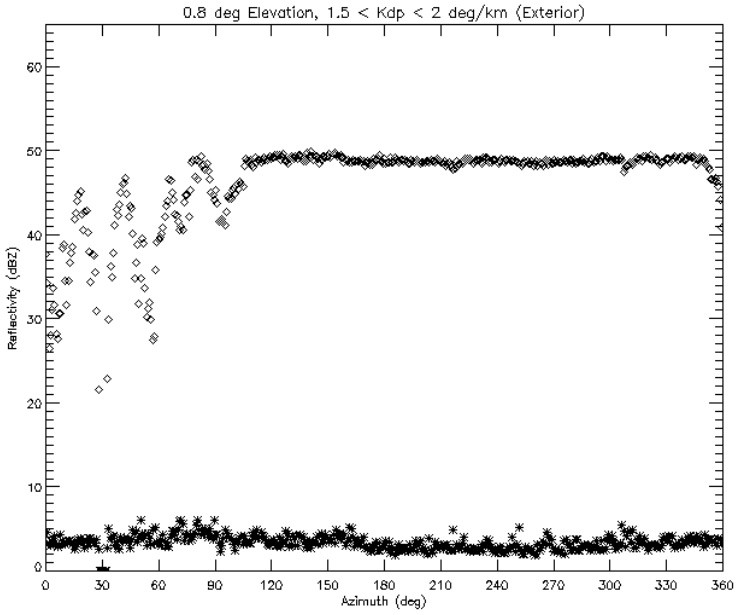

Figure 4. Median Z_H in rain as a function of azimuth for the indicated elevation and K_{DP} range (diamonds). Also shown is standard deviation in Z_H (*). This plot used S-Pol data throughout the NAME EOP and is for exterior ranges.

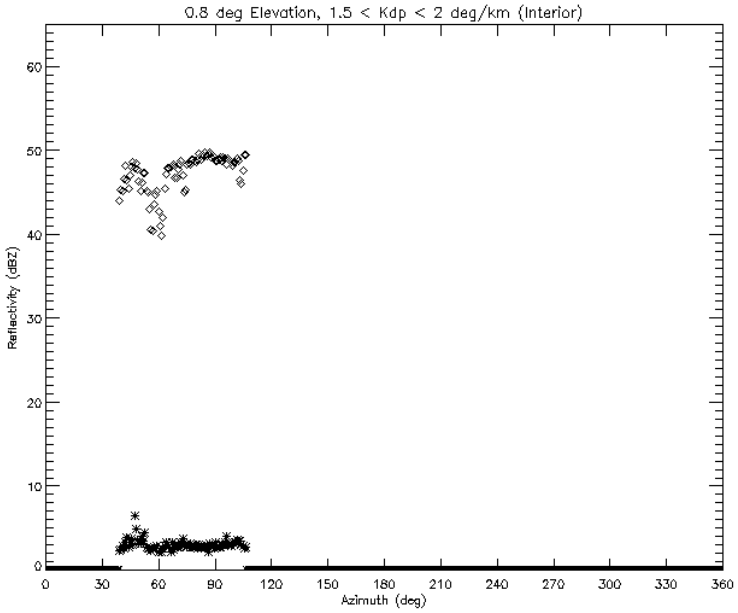

Figure 5. Median Z_H in rain as a function of azimuth for the indicated elevation and K_{DP} range (diamonds). Also shown is standard deviation in Z_H (*). This plot used S-Pol data throughout the NAME EOP and is for interior ranges. Note that interior blocks only existed at a subset of angles.

However, in major blocks near 30° and 56° there was near total signal loss at 0.8°. Blockage was an issue, and was corrected for any sweeps up to 2° elevation. Each elevation's blockage was analyzed and treated separately.

We performed limited intercomparisons of correrected S-Pol Z_H with TRMM satellite overpasses. Figure 6 shows an example of this intercomparison. S-Pol data were interpolated to the same horizontal grid as the native TRMM Precipitation Radar (PR) data. The quality-controlled PPI sweeps closest in time (within 1-2 minutes) to the overpass was chosen. To make an estimate of reflectivity at each gridpoint, it was required that at least 8 ground radar gates had meterological data and were within 5 km horizontally and 250 m vertically of the PR gridpoint location. There is a high variance in the distribution of PR-GND Z values, which is expected given the radically different radar types, beam and scan geometries, etc. But the mean value of corrected S-Pol Z_H data is within 0.06 dBZ of TRMM PR, suggesting that the blockage correction (along with other reflectivity corrections; e.g., for attenuation) did an excellent job.

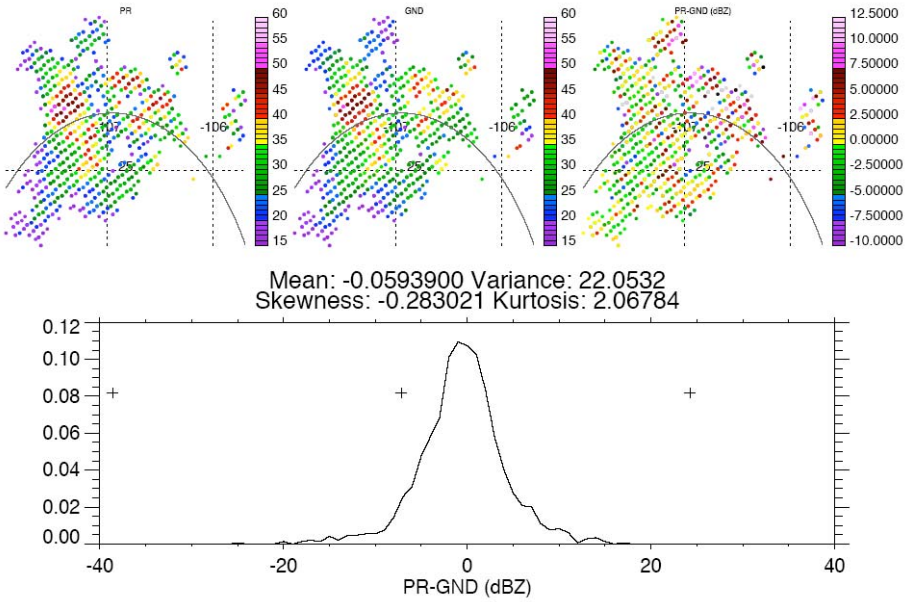

Figure 6. Maps of TRMM PR, corrected S-Pol (GND), and PR-GND Z_H values, along with a distribution of PR-GND, for a single TRMM overpass. The curve in the maps is an S-Pol range ring, indicating the radar was roughly SSW of the map center. The NE sector of S-Pol, corresponding to the eastern portions of the maps, was affected by beam blockage.

We corrected blocked Z_{DR} at blocked elevations using the methodology of Giangrande and Ryzhkov (2005). Here we examine Z_{DR} variability in drizzle (as defined by the CSU HID algorithm) as a function of azimuth. Figure 7 shows an example for exterior ranges.

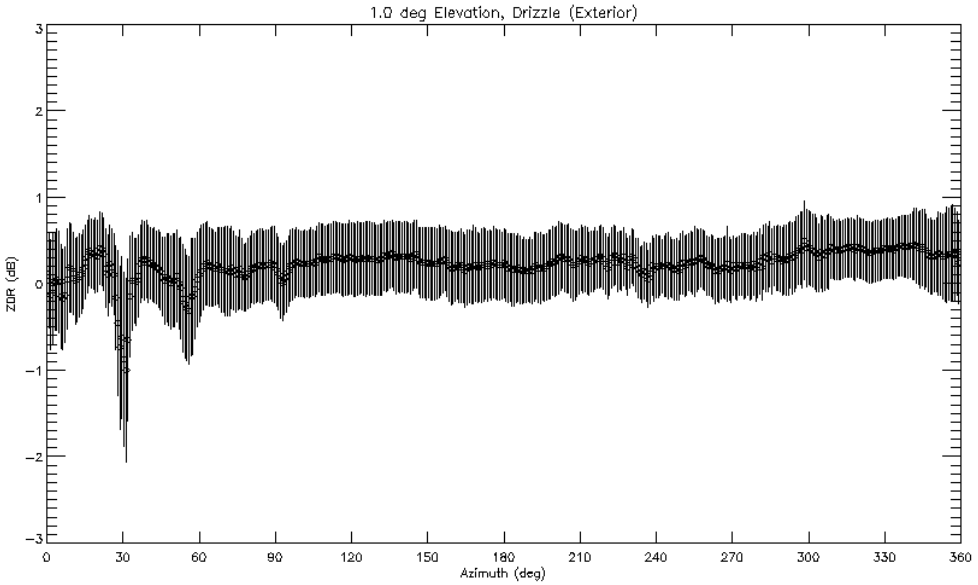

Figure 7. Median Z_{DR} in drizzle as a function of azimuth for the indicated elevation (require K_{DP} < 0.1; diamonds). Also shown is standard deviation in Z_{DR} (error bars). This plot used S-Pol data throughout the NAME EOP and is for exterior ranges.

4.0 DATA FORMAT

INTRODUCTION

We produced 3-D latitude/longitude/height grids approximately every 15 minutes from the S-Pol radar, situated near the mouth of the Gulf of California in summer 2004. The following fields were created:

DB	(reflectivity in dBZ)
LD	(linear depolarization ratio in dB)
RH	(correlation coefficient at 0 lag)
ZD	(differential reflectivity in dB)
KD	(specific differential phase in ° km^{-1})
HI	(hydrometeor identification tag)

HI values refer to the following dominant (reflectivity-wise) hydrometeor species in a particular gridpoint: 0 – unclassified, 1 – drizzle, 2 – rain, 3 – dry snow, 4 – wet snow, 5 – vertically aligned ice crystals, 6 – low-density graupel, 7 – high-density graupel, 8 – small hail (diameter D < 2 cm), 9 – large hail (D > 2 cm). The methodology used to determine these categories, as well as their interpretation, was identical to Tessendorf et al. (2005).

In all fields, the missing_value assigned to grid points with no echo or scan coverage was -99999.

The array size for each grid is 165x165x20. The horizontal grid spacing is 0.02° lat/lon (~2 km). The grid spans –108.6° to –105.32° in longitude and 22.28° to 25.56° in latitude. The grid matches with the 2-D regional composite grids (Lang et al. 2007) for easy intercomparison. In an array system where (i,j)=(0,0) is the lower left (SW) corner of the 2-D regional composite map, the 3-D grids span i=225-389 and j=124-288. Use these ranges of indices when matching the 3-D grids to the 2-D regional composites.

The vertical grid spacing is 1 km. The first altitude level is 1 km MSL, so the grids cover 1-20 km MSL.

Filenames denote the UTC date and time for start time of the radar volume from which each grid was derived (filename format: ufd.1YYMMDDHHMMSS.SPOL.0.nc).

GRIDDING METHODOLOGY

The grids were created using NCAR's Sorted Position Radar INTerpolator (SPRINT; Mohr and Vaughn 1979; Miller et al. 1986). Prior to interpolation, the data were filtered using SPRINT's FILTER command. A Cressman filter with a radius of 10 gates in range and 1 beam in azimuth was used. Data were gridded using the GRIDLLZ command. All decibel fields (DB, LD, ZD) were linearized prior to filtering and gridding. Hydrometeor identification (HI) was performed after gridding, using a project-mean temperature sounding from Mazatlan.

We used SPRINT because it allowed easy gridding in lat/lon, as opposed to NCAR's REORDER package. SPRINT has some limitations, however. One is that gridded echo does not extend as far out in range as the viewable radar scan. The origin of this problem is unknown, but it is not a big factor because gridded echo extends to ~160 km range, beyond which vertical resolution is very poor anyway. The other problem is that SPRINT's FILTER command is very rudimentary and does not allow a direct method of having a variable radius of influence in the vertical. These leads to some ring effects in the grids.

Output format: NetCDF
For more info about NetCDF, see http://my.unidata.ucar.edu/content/software/netcdf.

Here is an example header dump using ncdump:

```
netcdf ufd.1040805061508.SPOL.0 {
dimensions:
        x = 165 ;
        y = 165 ;
        z = 20 ;
variables:
        float DB(z, y, x) ;
                DB:missing_value = -99999.f ;
        float LD(z, y, x) ;
                LD:missing_value = -99999.f ;
```

```
        float RH(z, y, x) ;
                RH:missing_value = -99999.f ;
        float ZD(z, y, x) ;
                ZD:missing_value = -99999.f ;
        float KD(z, y, x) ;
                KD:missing_value = -99999.f ;
        float HI(z, y, x) ;
                HI:missing_value = -99999.f ;
        float x(x) ;
                x:longname = "Distance E/W [long]" ;
                x:units = "deg" ;
        float y(y) ;
                y:longname = "Distance N/S [lat]" ;
                y:units = "deg" ;
        float z(z) ;
                z:longname = "Height [km]" ;
                z:units = "km" ;

// global attributes:
                :ident = "SPOL  " ;
                :title = "Cartesian data from SPOL   at 4/8/5 6:15:8" ;
                :xname = "Distance E/W [long]" ;
                :xfirst = -108.6f ;
                :xdelta = 0.02f ;
                :xunits = "deg" ;
                :yname = "Distance N/S [lat]" ;
                :yfirst = 22.28f ;
                :ydelta = 0.02f ;
                :yunits = "deg" ;
                :zname = "Height [km]" ;
                :zfirst = 1.f ;
                :zdelta = 1.f ;
                :zunits = "km" ;
}
```

5.0 DATA REMARKS

Figure 8 shows periods of PPI sector scanning by S-Pol. These periods will have less than the full 360° volume covered by the radar (usually 90-120° only). Keep this in mind when interpreting or analyzing volumes from these time periods.

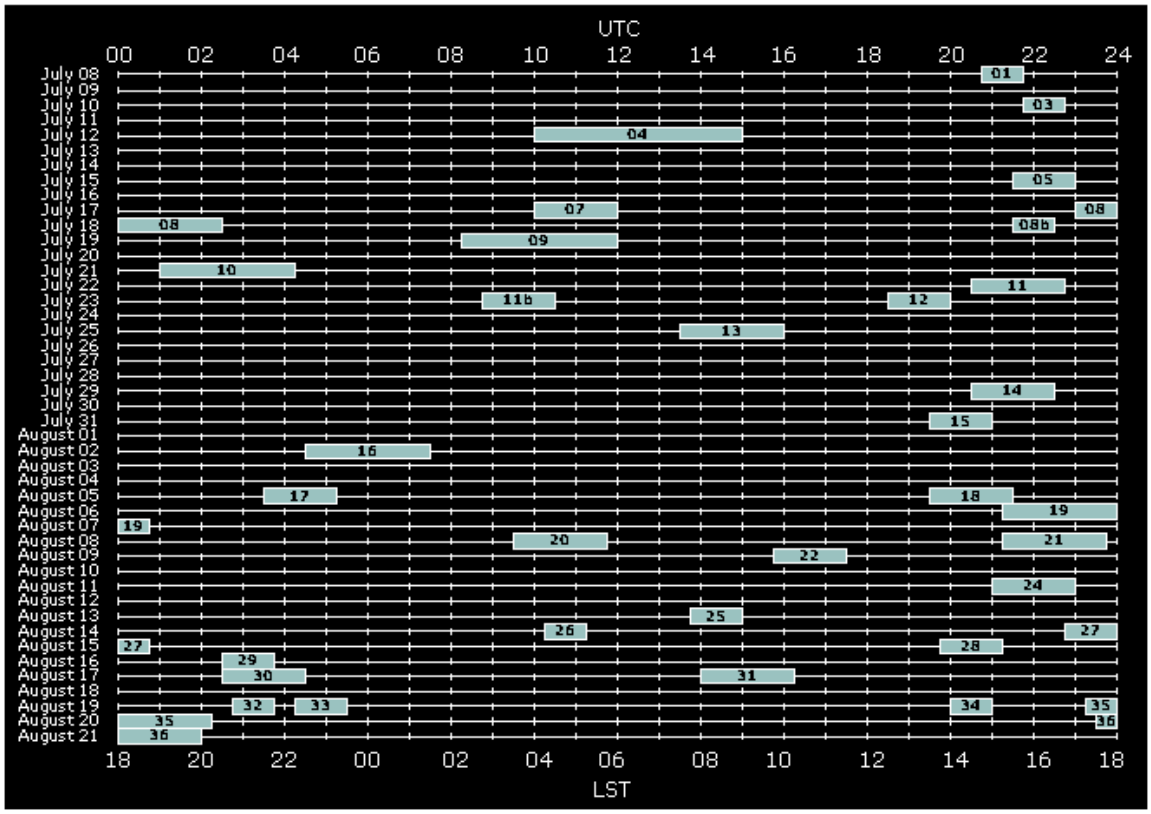

Figure 8. Periods of high-resolution S-Pol scanning (light blue bars) during the NAME EOP, labeled by case number. Top abscissa is UTC, bottom is local time (UTC minus 6 h).

6.0 REFERENCES

Battan, L. J., 1973: *Radar Observation of the Atmosphere*. University of Chicago Press, 324 pp.

Bringi, V. N., and V. Chandrasekar, 2001: *Polarimetric Doppler Weather Radar: Principles and Applications*. Cambridge University Press, 636 pp.

Doviak, R. J., and D. S. Zrnic, 1993: *Doppler radar and weather observations.* Academic Press, 562 pp.

Giangrande, S. E., and A. V. Ryzhkov, 2005: Calibration of dual-polarization radar in the presence of partial beam blockage. *J. Atmos. Oceanic. Technol.*, **22**, 1156-1166.

Lang, T. J., D. A. Ahijevych, S. W. Nesbitt, R. E. Carbone, S. A. Rutledge, and R. Cifelli, 2007: Radar-observed characteristics of precipitating systems during NAME 2004. *J. Climate*, **20**, 1721−1741.

Miller, L.J., C.G. Mohr, and A.J. Weinheimer, 1986: The simple rectification to Cartesian

space of folded radial velocities from Doppler radar sampling. *J. Atmos. Oceanic. Technol.*, **3**, 162-174.

Mohr, C.G., and R.L. Vaughn, 1979: An economical approach for Cartesian interpolation and display of reflectivity factor data in three-dimensional space. *J. Appl. Meteor.*, **18**, 661-670.

Tessendorf, S. A., L. J. Miller, K. C. Wiens, and S. A. Rutledge. 2005: The 29 June 2000 supercell observed during STEPS. Part I: Kinematics and microphysics. *J. Atmos. Sci.*, **62**, 4127–4150.